Visibility of stars, halos, and rainbows during solar eclipses

Gunther P. Können[1,*] and Claudia Hinz[2]

[1]Sophialaan 4, NL-3761DK Soest, The Netherlands

[2]Deutscher Wetterdienst, Bergwetterwarte Wendelstein, D-83735 Bayrischzell, Germany

*Corresponding author konnen@planet.nl

Received 27 February 2008; revised 22 May 2008; accepted 22 May 2008;
posted 22 May 2008 (Doc. ID 93011); published 13 June 2008

The visibility of stars, planets, diffraction coronas, halos, and rainbows during the partial and total phases of a solar eclipse is studied. The limiting magnitude during various stages of the partial phase is presented. The sky radiance during totality with respect to noneclipse conditions is revisited and found to be typically 1/4000. The corresponding limiting magnitude is +3.5. At totality, the signal-to-background ratio of diffraction coronas, halos, and rainbows has dropped by a factor of 250. It is found that diffraction coronas around the totally eclipsed Sun may nevertheless occur. Analyses of lunar halo observations during twilight indicate that bright halo displays may also persist during totality. Rainbows during totality seem impossible. © 2008 Optical Society of America

OCIS codes: 010.2940, 010.1290, 350.1260.

1. Introduction

We discuss the visibility of stars and planets during partial and total solar eclipses and the occurrence of rainbows, halos and diffraction coronas during eclipses. The discussion brings together studies of sky brightness during eclipses, studies of limiting magnitudes under various conditions, and visibility studies in meteorological optics. In all of these fields there exists a vast amount of literature, but to our knowledge these areas are rarely combined. With respect to sky brightness data during totality, the basic sources are the overview articles from the 1970s by Sharp *et al.* [1], Silverman and Mullen [2], as well as the summarizing work by Dandekar [3], Shaw [4], and others. Extensive studies of limiting magnitudes—the stellar magnitude of the faintest point source that can be seen against a luminous background—in the laboratory, during twilight, and during daytime, were performed during the 1940 and 1950s, most notably by Blackwell [5], Lamar *et al.* [6], Hecht [7], Tousey and Hulburt [8,9], Weaver [10], Koomen *et al.* [11], and Tousey and Koomen [12]. The gained knowledge of limiting magnitudes has been only meagerly applied to eclipses. Silverman and Mullen [2], in discussing star sightings during totality, remark that the limiting magnitude is about +3 and add to this that, indeed, on a few occasions third magnitude stars have been observed, but that these observations are the result of chance rather than of deliberate attempts at star observations. Despite his call for systematic pursuits of stars during totality, little progress has been made since.

The appearance of phenomena from meteorological optics—diffraction coronas, halos, and rainbows—during eclipses, and their capability to persist during totality has received even less attention. The unpredictability of their appearances obviously hinders the planning of systematic observation campaigns for these phenomena. In some recent cases, however, the required cirrus or altocumulus clouds have been present during totality together with keen observers on the ground. By virtue of these observations and the existence of long observational records of ordinary halos, it is now possible to assess their capability to remain visible during eclipses.

0003-6935/08/340H14-11$15.00/0

A crucial parameter in this study is $I_{tot}/I_{0\%}$, which is the sky brightness during totality with respect to the brightness under noneclipse conditions. Based on the authority of the two overview articles [1,2], one usually takes for this a value of 10^{-3}. Part of the present study is devoted to revisiting the literature on which the traditional value is based, which leads us to conclude that this value is about half an order of magnitude too high.

We split the paper into two parts. The first describes effects during the partial phase; the second during totality. Apart from sightings of stars, diffraction coronas, halos, and rainbows, some other real or psychophysical effects will be touched on in this paper.

2. Partial Phase

A. Eclipse Timeline

The time span between the first contact of the Moon and the start of totality (second contact) is typically 70–90 min. A central value is 80 min; this value is used in this paper to define the eclipse timeline. During this partial phase the magnitude of the eclipse, being the fraction of the solar diameter that is obscured by the Moon, increases about linearly with time. The obscuration of the Sun, which is the fraction of the surface area of the solar disc that is hidden by the Moon (and hence governs the attenuation of the light of the Sun), lags a bit behind in the beginning of the partial phase: after a half hour from the first contact the magnitude of the eclipse is already 0.4, but the obscuration only 29%. After this it accelerates: in the remaining 50 min to totality the obscuration increases almost linearly with the eclipse magnitude and hence with time [13]. See Table 1, in which the Sun's photometric brightness is calculated as a function of eclipse magnitude for a typical eclipse (ratio lunar/solar disk diameter 1.04). Limb darkening [14] is taken into account in Table 1, but its effect becomes apparent only for deep partial eclipses: for eclipse magnitudes of 0.8, 0.90, and 0.95 it causes an additional weakening of the Sun's radiance by 15%, 25%, and 35% respectively, amounting to about 50% just before totality. We note that the wavelength dependency of the limb darkening has little effect on the Sun's brightness, as it affects these weakening factors by less than 10% in the 500–600 nm range.

B. Human Perception of Attenuation

The reduction in illumination remains initially unnoticed by the human eye for three reasons. First, according to Fechner's law [15], the eye responds logarithmically to stimuli; second, the decrease in radiance of the blue sky and our surroundings is the same as that of the primary light source, so that contrasts remain unaffected; and third, just like a good camcorder, the eye adapts effectively to changes in the overall illumination. Rather than the light looking dimmer, one perceives that fixed light sources—like the planet Venus or a remote street light—seem to gain in brightness. Only when the eclipse magnitude exceeds 0.9, hence about 10 min before totality, does the continuous decrease of the light intensity start to become noticeable [16]. This happens when the rate of decrease in the light level has risen to 15%/min, which is comparable with the rate during ordinary [3,11,17–19] civil twilight. At that point, the absolute level of the illumination is already a factor of 10 less than at the beginning of the eclipse.

Via other human senses, the decrease in radiation is apparent much earlier. Almost everyone (see, e.g., [20]) experiences a chilling feeling at eclipse magnitude 0.6 (about a half hour before totality). Measurements show that the air temperature has dropped by less than 2 °C at that stage [21], which is not sufficient to explain this cold sensation. The explanation of this is that our temperature sensation is determined mainly by the Sun's radiation and hardly by the real temperature [22]: a decrease in direct Sun radiation from 100% to 75% creates (during still weather and temperatures around 15°C–25°C) a sensation similar to a temperature drop of no less than 5°C. Everyone knows indeed how strong the effect can be of a small cloud blocking the Sun: apparently our sense for cold is a much better detector for absolute radiation than our adapting eyes.

When the eclipse magnitude exceeds 0.9, observers start to perceive a bluish hue in the sky and landscape. Reports of it date back to the 19th cen-

Table 1. Obscuration and Brightness of the Partially Eclipsed Sun for Wavelength 550 nm and Moon/Sun Diameter Ratio 1.04

Eclipse Magnitude[a]	Time till Totality	Obscuration[b]	Brightness Sun[c]	Stellar Magnitude Sun[d]
0	80 min[e]	0	100%	−26.70
0.1	72 min	4%	97%	−26.67
0.2	64 min	11%	91%	−26.60
0.3	56 min	19%	82%	−26.49
0.4	48 min	29%	72%	−26.34
0.5	40 min	40%	60%	−26.14
0.6	32 min	51%	47%	−25.88
0.7	24 min	63%	34%	−25.52
0.8	16 min	76%	21%	−24.99
0.85	12 min	82%	15%	−24.60
0.9	8 min	88%	9%	−24.04
0.95	4 min	94.6%	3.5%	−23.05
0.975	2 min	97.6%	1.3%	−22.02
0.985	75 s	98.7%	0.7%	−21.30
0.995	24 s	99.7%[f]	0.13%[f]	−19.48
0.998	10 s	99.93%[f]	0.03%[f]	−18.00

[a]Part of the solar diameter obscured by the Moon.
[b]Part of the solar surface area obscured by the Moon.
[c]Limb darkening factors [14] for 550 nm applied.
[d]For solar elevation 40°.
[e]Value varies somewhat between different eclipses.
[f]From obscuration of 99.7% the decrease in sky radiance stagnates with respect to that of the Sun [18,27].

tury [23] and continue till the present [20,24,25]. The effect is unexplained and is likely to be a physiological and psychological response to the low and decreasing light levels, perhaps in combination with the sensation of cold. The bluish tinge sensation is strong enough to be noticed by many [26].

Even for eclipse magnitudes exceeding 0.99 the eclipse phenomenology can be interpreted in terms of attenuated, but otherwise unchanged, sunlight [1]. Only if an obscuration of 99.7% is reached, that is less than 30 s before totality, the decrease in skylight radiance starts to stagnate with respect to that of the Sun [1,4,27].

C. Appearance of Planets and Stars

The sky radiance follows that of the primary source, the Sun. With the decreasing sky radiance, the limiting magnitude, being the stellar magnitude of the faintest star that can be seen, goes up. At full day, sea level, and clear air conditions, the limiting magnitude is typically −3.5 in the regions of the sky that are farther than ∼40° from the horizon [8,10,12]. This value is in concordance with the observational experience of G. P. Können that Venus can be quite easily spotted with the unaided eye during full day even when its brightness is less than −4.0 magnitude and the Sun is as high as 60° in the sky.

With the decrease in sky light during the course of the partial phase, the visibility of Venus improves. For point sources, however [5,9], the increase in limiting magnitude progresses slower than the decrease in sky brightness implies: a diminishing of the sky brightness by 5 magnitudes results in an increase of only 4 points in limiting magnitude [12]. Table 2 shows that Jupiter and Sirius appear no sooner than about 10 min before totality; about 2.5 min before totality the limiting magnitude crosses the zero level. Theory fits well with the observations, as in 2006 Mercury (+1.0 magnitude, elongation 25°) was reported to be visually observed during the last minute before totality [16,20].

Figure 1 summarizes the sky brightness and limiting magnitude data during the last 2 min before totality. The representation is that developed by Sharp [1], who expresses the sky brightness I relative to that at obscuration 98.7%. At that point, the brightness of Sun and sky has decreased with respect to noneclipse conditions by a factor of 144 (for wavelength 550 nm and Moon/Sun radius 1.04), but the Sun's role as primary light source remains unchanged. The right axis shows the sky brightness with respect to noneclipse conditions $I/I_{0\%}$, where the factor 144 is used to derive their values from the $I/I_{98.7\%}$ values. Bars indicate the sensitivity of the factor 144 to variations in wavelength (±8%) and eclipse magnitude (±3%). The limiting magnitudes and the moments of appearance of the nine brightest stars that are closer than 25° to the ecliptic are added to the right-hand axis. The solid line represents the attenuation of sunlight; the dashed line indicates the decrease in brightness of the sky, which starts to deviate from that of the Sun [1,4,27] for an obscuration of 99.7%.

D. Diffraction Coronas, Halos, and Rainbows during the Partial Phase

Contrary to the situation for point sources, the visibility of light sources with sizes exceeding ∼0.3° depends, for sky radiances down to civil twilight, only on the signal-to-background ratio [5,6,9]. Because up to an obscuration of 99.7% the intensities of sunlight and sky light are attenuated in the same way, the signal-to-background ratio of diffraction coronas, halos, and rainbows generated by the light of the partially eclipsed Sun remains constant. This implies that up to that point the visibility of these objects remains unchanged. In the last 30 s before totality the signal-to-background ratio starts to worsen as the attenuation of the sky retards, but till the very last stage of partiality the Sun keeps its position as the prominent light source in the sky. As long as the scattering particles are directly lit, diffraction coronas, halos, and such can persist without significant loss in visibility. This is illustrated in Fig. 2, taken 9 s before totality [28], where a pollen corona is formed around the last unobscured piece of Sun.

Table 2. Limiting Magnitudes during the Partial and Total Phases of an Eclipse

Eclipse Magnitude	Obscuration	Time till Totality	Limiting Magnitude[a]	Planets/Stars Visible
0	0%	80 min	−3.5	Venus
0.72	66%	23 min	−2.5	
0.888	86.8%	9 min	−1.5	Jupiter, Sirius
0.954	95.3%	3.7 min	−0.5	Canopus, Mercury
0.980	98.2%	97 s	+0.5	α Cen, Arcturus, Vega, Rigel, Capella, Procyon, Saturn
0.986	98.9%	65 s	+1.0	Achenar, β Cen, Altair, Aldebaran, α Crucis, Antares, Betelgeuse
0.991	99.4%	44 s	+1.5	Spica, Pollux, Fomalhaut, Deneb, β Crucis, Regulus
Mid-totality[b]	100%	—	+3.5	E.g., Alcyone in Pleiades cluster

[a]At clear sky and sea level.
[b]Limiting magnitude as derived in this work.

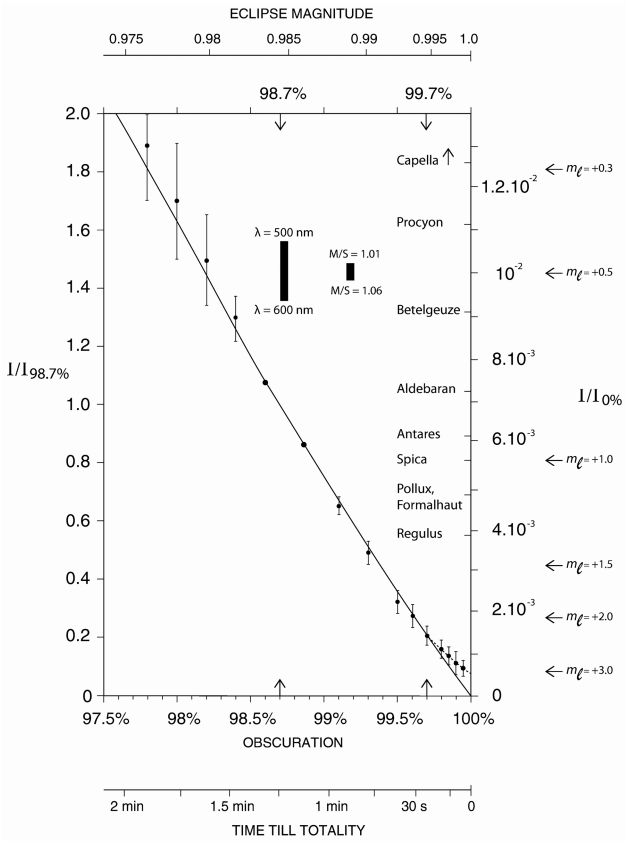

Fig. 1. Sky radiance I relative to that at 98.7% solar obscuration $I_{98.7\%}$ as a function of percent of obscuration. The solid line shows the brightness of the Sun relative to that at 98.7% solar obscuration for Moon/Sun radius 1.04 and wavelength 550 nm. The dots with the standard deviations are observed sky radiances, and the dashed line is a fit through these points as reported by Sharp [1]. The right-hand vertical axis represents the radiance relative to that at zero solar obscuration, $I/I_{0\%}$. The two solid bars show the respective variation of the 10^{-2} point of that axis for Moon/Sun radius (M/S) values ranging from 1.01 to 1.06 and for wavelengths from 500 to 600 nm. The limiting magnitudes (m_l) and the magnitudes of the nine stars that are closer than 25° to the ecliptic and brighter than magnitude 1.5 are added to that axis. Capella, the brightest among them, would fall on a $I/I_{98.7\%}$ value of 2.25.

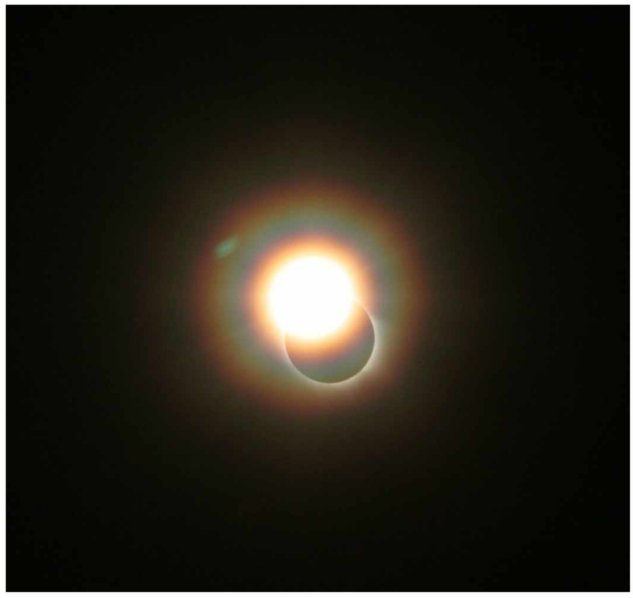

Fig. 2. (Color online) Pollen corona around the deeply eclipsed Sun, 9 s before totality. The solar obscuration is 99.92%. Even at this very last stage of partiality, the light of the Sun completely outshines that of the solar corona and determines the formation of the pollen corona (photo by Emma Herranen; Belek, south Turkey, 29 March 2006; see also [28]).

3. Totality

A. Transition to Totality

In a transition phase of about 30 s, the scene changes from directly sunlit to total eclipse conditions. In that time span the direct sunlight disappears, 10 s before still being of magnitude −18, to be replaced by the corona, of magnitude −12.0 [29–31]. The decrease in illumination continues after second contact is reached, as in the initial stage of totality part of the sky is still directly lit by the Sun (Fig. 3) and hence is relatively bright. The end of the transition phase occurs when the sunlit part of the sky has disappeared behind the horizon.

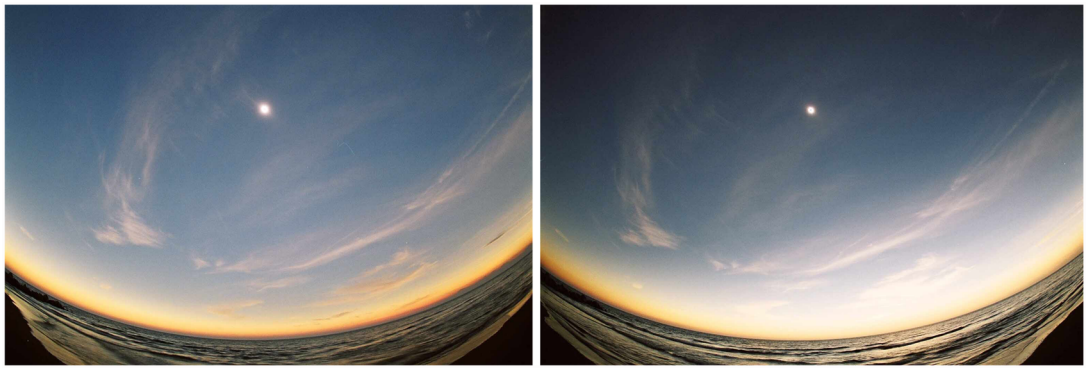

Fig. 3. (Color online) Left, the sky at mid-totality. Right, on the edge of totality, 10 s before third contact. The boundary between direct sunlit and the indirectly lit air mass has approached the Sun to 30°. This boundary line is sharply visible because we are looking almost parallel to the lunar umbra. Fisheye lens, horizontal field of view 135° (photos G.P. Können, at 3.7 km NW of the center line of totality; Side/Colakli, south Turkey, 29 March 2006).

Visually, the transition phase represents a strong sensation of light dimming, which extends well into the initial stage of totality. This sensation is even stronger under an overcast sky, as G. P. Können knows from his experience during the 1999 Luxemburg and 2006 Turkey eclipses. The reason is that the time needed for the lunar umbra to cross the sky is shorter if the effective scattering height is lower, which is the case under a cloud deck. The visual transition phase during the overcast eclipse in Luxemburg of 1999 lasted only 10 s, in agreement with the data of a fixed-diaphragm video by Rob van Dorland [32]; the visual transition phase during the 2006 Turkey eclipse was three times longer.

At second and third contacts the boundary between directly and indirectly lit air masses passes straight through the Sun. Because we are looking parallel to the lunar umbra, it is instantly visible as a sharply defined line in the sky. In Fig. 3 (right), taken 10 s before third contact, there is a gradient in sky radiance of a factor of 4 in a 20° interval across the boundary. In the regions of the sky where the boundary is clearly defined, the drop in radiance during the transition to totality may be much steeper than radiance measurements of the zenith sky [3,18,27,33,34] suggest.

Figure 3 also illustrates that the brightness variation of the zenith sky need not coincide with that of the Sun: in this particular case, the former lagged behind. This effect may partly explain the observed asymmetries with respect to the time of mid-totality in instrumentally recorded light curves of the zenith sky [1,4,35–37].

The factor of 4 sky radiance difference across the lunar shadow implies that light on the sunlit site of it consists of 75% primary scattered light and 25% multiply scattered light. This quantifies the loss in the signal-to-background ratio of halos and diffraction coronas and such during the very last stage before totality. As the radiance of halos or diffraction coronas from sunlit particles is proportional to that of the primary scattered component of sky light, this indicates that the signal-to-background ratio of these near-Sun phenomena has dropped by no more than 25% with respect to noneclipse conditions. In accordance with Fig. 2 and the Hennig halo discussed below, this implies that the visibility of these phenomena remains remarkable stable till the moment that the umbra reaches them.

When the sunlit part of the sky has disappeared and totality is stabilized, the brightness of the sky is comparable with twilight, or solar depression angle 5°–7° ([1,3,18,19,27,33,35,38]; see also [4]), hence like at the end of ordinary civil twilight. This means that the light level remains high enough to keep the human eye in the region of photoptic (cone) vision. The light distribution in the sky is remarkably smooth [4]. For zenith distances z less than 70°, its main features can be well understood from second-order scattering modeling [39–41], in which the dependence of the light distribution turns out [39] to be basically proportional to the path length factor $1/\cos(z)$. For understanding the region closer to the horizon, single scattering has to be invoked [42]. The two eclipse overview articles [1,2] indicate the loss in sky radiance with respect to noneclipse conditions to be 3 orders of magnitude. Other sources [3,4,18,33,34] as well as theoretical modeling [39,41] indicate that this value is on the conservative side.

The most prominent light source in the sky is the solar corona. With a brightness of −12.0 magnitude it stands out against the sky like the Moon at phase 0.93 (elongation 150°) against a twilight sky at solar depression angle 5°–7°. In that situation, the contribution to the irradiance by the corona light is negligible with respect to that of the sky [41]. Hence the corona, like the Moon during civil twilight, casts no shadows.

B. Appearance of Stars and of the Eclipsing Moon

Figure 4 summarizes sky brightness observations during totality. Again the sky radiance is expressed relative to that at obscuration 98.7%. The figure contains 16 data points of eclipse observations from ground level (less than 500 m above sea level) with solar elevation higher than 20°. These include six data points from Fig. 2 of [1]. Details are given in Table 3. The observations refer often, but not always, to the zenith. The right axis of Fig. 4 shows the sky brightness with respect to noneclipse conditions $I_{\mathrm{tot}}/I_{0\%}$, where the above-mentioned factor 144 is used to derive their values from the $I_{\mathrm{tot}}/I_{98.7\%}$ values. The limiting magnitudes corresponding to the right-hand axis, as derived from Fig. 1 of [12], are indicated. They can be considered to be representative for regions in the sky that are higher than ∼40° from the horizon.

The data in Fig. 4 indicate a typical value of $I_{\mathrm{tot}}/I_{98.7\%}$ of about 0.035. This indicates a central estimate for $I_{\mathrm{tot}}/I_{0\%}$ of 1/4000, which fits the data points within a factor of 2. This implies that the loss in sky radiance with respect to noneclipse conditions is half an order of magnitude higher than the value recommended by Sharp *et al.* [1,2]. The 1/4000 value is in accordance with the values directly reported by the various observers in Table 3, as well as with the value calculated by the radiative transfer model [41]. It is also consistent with the radiance loss [8,11] of the sky from full day till solar depression angle 6°, and hence with the twilight equivalence of the sky at totality.

The factor 1/4000 implies a limiting magnitude of about +3.5. The gradient in radiance of a factor of 4 in an interval of 20° across the lunar shadow in Fig. 3 implies that the increase in limiting magnitude from +2.5 till its final value of +3.5 may progress almost stepwise.

Accepting that the value of +3.5 is not too far from the truth, a perfect object for future testing of the limiting magnitude during totality is the Pleiades cluster. The magnitudes 2.9, 3.6, 3.7, and 3.9 of its

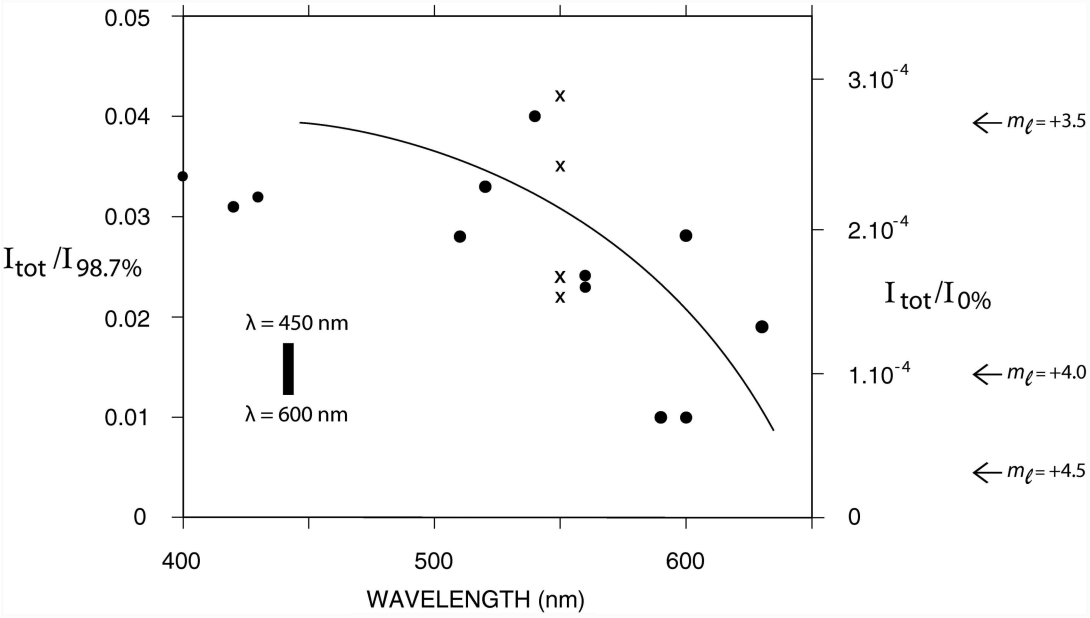

Fig. 4. Sky radiance I_{tot} during totality relative to that at 98.7% solar obscuration $I_{98.7\%}$ as a function of wavelength. The dots are narrow-band observations; the crosses, put at wavelength 550 nm, indicate broadband observations in the visible range (see Table 3). The right-hand vertical axis represents the radiance relative to that at zero solar obscuration, $I_{tot}/I_{0\%}$. The solid bar shows the variation of the 10^{-4} point of that axis for wavelengths from 450 till 600 nm. The limiting magnitudes (m_l) corresponding to the sky radiances is added to that axis. The solid line is a rough fit through the data.

four brightest stars cover well the uncertainty range of the limiting magnitude during totality.

Next to the solar corona and the planet Venus, the brightest object in the sky is the eclipsing Moon. The earthshine on the new Moon makes it an object of magnitude −3.0, as can easily be calculated from the brightness of the full Earth as seen from the Moon (−16.9) and the value (30%) of the Moon's opposition effect [45–47]. The factor 1/4000 implies that the signal-to-background ratio is the same as that for the easily observable gibbous Moon at full day. Nonetheless, the human eye perceives an ink-black disk instead. The cause is the contrast with the bright corona. The black disk illusion (Fig. 5) is among the strongest optical illusions that exists [48].

C. Diffraction Coronas, Halos, and Rainbows during Totality

1. *General*

As the radiance of the solar corona is 10^6 times weaker than the uneclipsed Sun, whereas the sky radi-

Table 3. Sky Brightness at Totality

Year (Eclipse Magnitude [43])	Solar Elevation	Wavelength	$I_{tot}/I_{98.7\%}$	$I_{tot}/I_{0\%}$ Reported	Observer, Remarks
1937 (1.075)	30°	visible	0.024[a]		Richtmyer [31]
1947 (1.056)	40°	visible	0.035[a]	1/4000	Richardson and Hulburt [37]
1952 (1.037)	61°	visible	0.042[a]		Batchelder *et al.* [36]
1963 (1.022)	24°	560 nm	0.023[a]		Sharp *et al.* [18]
		520 nm	0.033[a]	1/3500	
		600 nm	0.010[a]		
1966 (1.023)	68°	540 nm	0.040	1/2500	Lloyd and Silverman [34]
1970 (1.041)	37°	430 nm	0.032		Hall [44]
		510 nm	0.028		
		590 nm	0.010		
1970 (1.041)	46°	420 nm	0.031	1/7300	Dandekar and Turtle [33]
		560 nm	0.024	1/6400	
		630 nm	0.019	1/5800	
1973 (1.072)	37°	400 nm	0.034		Shaw [4], solar vertical, 90° from the Sun
		midvisible	0.022[b]		
		600 nm	0.028	1/7500	

[a]Values derived by Sharp [2].
[b]Value reported by Shaw [4].

Fig. 5. (Color online) Black disk illusion. The eclipsing Moon shows up to the human eye as black. Pasting a copy of its image against the sky shows its actual brightness with respect to the sky (magnification of a photo from C. Brinkerink; Side, south Turkey, 29 March 2006).

ance during totality has dropped only by a factor of 4000, the signal-to-background ratio of diffraction coronas, halos, and rainbows generated by the light of the corona is 250 times less than during noneclipse or pretotality conditions. It is not clear beforehand to what degree solar-corona generated phenomena of this type can stand out against the background light of the sky during totality.

2. *Diffraction Coronas during Totality*

Despite the poor signal-to-background conditions, the diffraction corona, being the brightest among these three phenomena, has indeed regularly been observed around the totally eclipsed Sun, and in 1999 even photographed. The first person who managed to obtain an unequivocal picture of a diffraction corona around the totally eclipsed Sun seems to be the Dutch observer Monique van Boxtel; her picture is reproduced as Fig. 6. Inspection of videos taken by others during totality reveals that in some of them

Fig. 6. (Color online) Diffraction corona around the totally eclipsed Sun. The light of the solar corona turns out to be sufficiently strong to produce a diffraction corona, which stays visible against the twilightlike background of the sky during totality (photo by Monique van Boxtel; Gmunden, Austria, 11 August 1999).

diffraction coronas can also be discerned, like for instance in the video taken by Anton van der Salm [49] during the 1991 Mexican eclipse. These videotaped diffraction coronas are usually much more difficult to recognize than the one in Fig. 6. A main reason for this is that eclipse photographers usually apply big telephoto lenses that tend to overmagnify a diffraction corona.

In the course of the 20th century, a few other eclipse watchers have reported the sighting of a diffraction corona around the totally eclipsed Sun [50], but we never saw pictures of them published. Perhaps the disappointment about the spoiling presence of the diffraction-corona-generating clouds during totality is sometimes too great to appreciate the effect. In some cases the diffraction corona has been observed but not recognized as such, like in 1998 when it was mistakenly identified as a possible (bluish) extension of the solar corona at 3.5° of the Sun [48].

3. *Halos during Totality*

Halos are weaker than diffraction coronas. It is not immediately clear whether the visibility of halos can withstand the dramatic loss in the signal-to-background ratio that occurs at totality. Reports about eclipse halos are lacking, although the German halo observer Udo Hennig saw and photographed a 22° halo that remained visible till 3 s before the totality of the 2006 eclipse (Fig. 7). After the beginning of totality this halo submerged in the background light of the sky, as could be testified by Hennig's two pictures that were taken during totality. The return of the halo could not be verified, as no posttotality pictures were taken. Hennig's series of pictures started 5 min before totality (at obscuration 92%), and his eight pictures taken during the increasing deeper partiality confirm our conclusion in Subsection 3.A that the signal-to-background ratio of a halo generated by a partially eclipsed Sun remains virtually constant till the very last moments before totality. However, Hennig's observation gives no indication as to how far the visibility of halos can survive the transition to totality, as this particular halo, which G. P. Können happened to see at about 300 m from Hennig's spot, was only of mediocre brightness.

To test whether brighter displays may persist during totality, we analyzed the lunar halo observations during twilight in the 21-year database of the German Halo Network (AKM, Arbeitskreis Meteore [51]). The introduction of lunar halos as an analogy of solar-corona-induced halos is justified by the fact that the smearing of a halo by the ~1°-wide solar corona is still small with respect to a halo's typical width and diffraction broadening [52]. At elongation 150° (phase 0.94), hence 30° from full, the brightness of the Moon equals that of the solar corona, while the sky radiance during totality roughly approximates twilight conditions for a solar depression angle of about 5°–7° (or $6° \pm 1°$). Using the brightness data of the Moon [53] as a function of elongation and

Fig. 7. (Color online) Left, 22° halo of mediocre brightness around the deeply eclipsed Sun, about 3 s before totality. The lunar shadow, approaching from the right bottom (see Fig. 3) has not yet reached the halo. At totality, the halo disappeared in the background illumination (photo by Udo Hennig; Side/Colakli, south Turkey, 29 March 2006, 10:54:52 UT). Right, 22° halo around the uneclipsed Sun. Owing to its extreme brightness this halo attracted wide attention. If the Hennig halo had been as bright as this one, it might have stayed visible during the total phase of the eclipse (photo by Dorothé Trompert; Alice Springs, Australia, 15 November 2005 13:17 LT).

the radiance of the twilight sky as a function of solar depression and the Moon's position in the sky [11,12], we determined, for values of lunar elongation other than 150°, the solar depression angle at which the Moon/sky radiance ratio equals that of the Moon at elongation 150° (phase 0.94) and solar depression angle 6°. For instance, for the Moon in first quarter, where its radiance is a factor of 5 less than at elongation 150°, this happens when the solar depression is 7.6° (Fig. 8), which occurs in the mid-latitudes about 45 min after sunset. Hence a halo that appears around the Moon in first quarter while the Sun is 7.6° below the horizon would have the same signal-to-background ratio as if that halo had appeared around the Moon at elongation 150° and solar depression angle 6° as well as if it had appeared around the totally eclipsed Sun under nominal eclipse conditions. Then we plotted the lunar phase and the solar depression of the evening lunar 22° halos in the AKM database that are observed before the end of nautical twilight (solar depression less than 12°) as well as the band of conditions equivalent to elongation 150° and depression angle 6° with a 1° range around it. This was done after a rigorous data selection (Appendix A). The resulting plot is shown as Fig. 8.

It turns out that 14 out of the 168 data points in Fig. 8 are in the band or on the left-hand side of it, whereas the left-hand boundary of the remaining 154 dots roughly follows the shape of the right-hand side of the band. In the case of these 14 points, their position in the plot indicates that the observed halo would have had an equal or better signal-to-background ratio if it had appeared around the eclipsed Sun instead of around the Moon. These 14 points are from the data of 5 of the 9 observers responsible for the dots in Fig. 8. They all refer to situations in which the Moon stood well above the horizon: only in one case was the lunar height below 34°, while averaged over all 14 observations the lunar elevation turns out to be 47°. Coding errors in date and/or time may have caused dots to shift from the point cloud toward the left, but it seems unlikely that such an effect applies to all of these 14 outlying dots. So at least some of them seem real.

Our conclusion from Fig. 8 is that halos that are generated by the light of the solar corona are not always doomed to disappear in background light of the sky during totality, but may in some cases stay visible. This conclusion is based not only on the existence of the 14 outlying points, but also on the proximity of the edge of the point cloud of the remaining 154 dots to the band, in combination with the conservative nature of the graph when used as diagnostic for the appearance

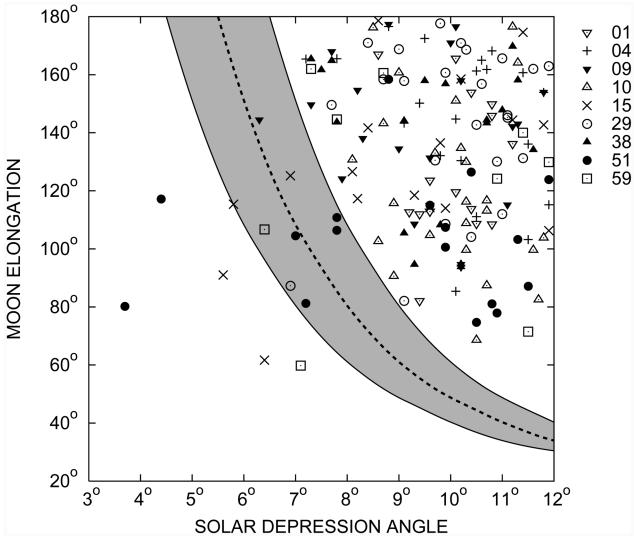

Fig. 8. Lunar 22° halo recordings during evening twilight as function of solar depression angle and lunar elongation (90° is first quarter; 180° is full Moon). The dashed curve indicates the situation in which the signal-to-background ratio is the same as that for a solar-corona-generated halo during totality for a nominal eclipse; the band around it indicates the range. Dots in the band or on the left side of it indicate observations for which the halo/sky radiance ratios were lower than when that halo would have been present during the totality of a typical solar eclipse. The presence of dots in that region indicates that halos could persist during the totality. The observations are by the Halo Network of the Arbeitskreis Meteore e.V, Germany, 1986–2006 (see Appendix A).

of halos during totality (see Appendix A). Future observations during the transition from the partial phase to totality are needed to experimentally find out to what extent bright halos can survive the 2–3 order of magnitude loss in signal-to-background ratio and to confirm their persistency during totality.

4. *Rainbows during Totality*

Rainbows are much weaker than halos. Given the just-mentioned analogy to the light conditions during twilight, it seems almost impossible that rainbows that are created by the light of the corona could ever be bright enough to rise over the sky background. Nonetheless, in 1970 a quite far-reaching claim about the visibility of eclipse rainbows appeared in the British journal *Weather* [50]. How far this claim can be taken seriously is questionable. The motivation to write this article was apparently a Letter to the Editor by the British Princess Margaret to the magazine *Country Life* about a lunar rainbow, and this fact may have prompted the author of the *Weather* article to make a somewhat stronger statement than the facts justify. Critical inspection of the eclipse report that forms the basis of this claim (from 1901, by Maunder [54]), shows that the bow was not observed by the author, but by a group 20 km away. Hence the information is only second hand, and the report contains no explicit indication that the bow persisted during the totality. The observed pink color in the bow, which Maunder suggests it may be caused by the hydrogen emission lines of the prominences, can be easily explained by the presence of a supernumerary bow. Probably this "eclipse rainbow" is observed only during the partial phase. A rainbow during totality seems impossible.

4. Conclusions

Our analysis leads us to the following conclusions:

- For partial eclipses greater than 0.9, stars can become visible in the sky.
- The signal-to-background ratio of halos and diffraction coronas generated by a partially eclipsed Sun remains virtually constant throughout the entire partial phase.
- The radiance of the sky during totality is typically a factor 4000 lower than at noneclipse conditions.
- This central estimate is half an order of magnitude higher than the classical value.
- During totality, the signal-to-background ratio of solar-corona-induced diffraction coronas, halos, and rainbows is a factor 250 times smaller than during nontotality.
- The limiting magnitude during totality is about +3.5.
- The Pleiades represent a very suitable object to observationally test the limiting magnitude during totality.
- Diffraction coronas are bright enough to stay visible during totality.
- Intrinsically bright halos also seem to be capable of remaining visible during totality.
- Rainbows during totality seem impossible. An opposing report probably refers to a rainbow during the partial phase.

Appendix A: Selection and Data Handling of Twilight Halos

The observational data that forms the basis of Fig. 8 are from the Halo Section of the Arbeitskreis Meteore e.V (Working Group Meteors, abbreviated AKM [51]), which is the organization that coordinates and documents the halo observations in Central Europe. This group, based in Germany, on 1 January 1979 introduced a systematic coding system (developed by Andre Knöfel and Gerhard Stemmler) for halo observations [55,56]. This system is of a structure similar to the coding used in the worldwide exchange of synoptic weather observations. The coded elements include the identification number of the observer, the date, the place of observation (home, work, or elsewhere), the halo-generating light source, the day of observation, the halo form, its brightness and a number of other halo-related details [57]. Two time indicators are coded: the moment that the halo was first seen, and the duration of the halo. The time of first appearance is always coded in Central European Time (CET, GMT + 1), regardless whether daylight saving time is effective, and regardless of the time zone where the observer happens to stay. In most cases, the time of first appearance is rounded to the nearest 5 min; the duration is given in units of 10 min. For twilight halos, these truncations can cause an error in solar elevation of maximally 0.4° at the first appearance but of 1.3° at the last appearance.

By the end of 2006, all observations from 1 January 1986 onward were put into the computer. At that point, the database contained over 65,000 observations. The number of observers per year grew from a dozen in the 1980s to more than 30 now. The coming and going of observers resulted in changes of observing points in the course of the years. In total, 78 observers contributed to the 1986–2006 database. Most of them live in Germany. The data selection proceeded in several steps.

First, AKM member Udo Hennig selected the 42 observers with more than 40 observations of lunar halos in their files and calculated the solar depression angles at the start, middle, and end of their observations. From these 42 files we deleted all observations that were done at places other than the observer's home, as well as all observation other than paraselenae and 22° halos around the Moon. As it turned out that lunar halo observations referred four times more often to the 22° halo than to paraselenae, we took the analysis further with 22° halo observations only, that being the only halo whose appearance is independent of lunar elevation angle. From this rarefied dataset we selected the files with at least 20 observations of lunar 22° halos during

nautical or civil twilight (solar depression angle 12° or less). This reduced the number of observers to 9, all of them living in Germany. These remaining observers and locations are Richard Löwenherz (town Klettwitz, identification number 01), Hartmut Bretschneider (Schneeberg, 04), Gerald Berthold (Chemnitz, 09), Jürgen Rendtel (Potsdam, 10), Udo Hennig (Radeberg, 15), Holger Lau (Pirna, 29), Wolfgang Hinz (Brannenburg, 38), Claudia Hinz (Brannenburg, 51), and the Weather Station Laage-Kronskamp (59). The geographical latitudes of these observers are typically between 51° and 53° N.

From this data set, we decided to use only the evening observations in the analysis. There are two reasons for that: first, the uncertainty in solar depression angle due to the truncations in time (see above) is lower; second, coding errors related to daylight saving time would result in underpopulation of events during evening twilight, but overpopulation of events during morning twilight. After this final selection and the deletion of double observations in the series of the couple Hinz (10 in total), there remained 168 observations at a solar depression angle of 12° or less; 83 of them are taken at a solar depression angle of 10° or less, 26 of them are taken at a solar depression angle of 8° or less, and 4 of them are taken during civil twilight (solar depression 6° or less).

It should be noted that the picture that arises from Fig. 8 about the visibility of eclipse halos—that is, where the solar corona has taken over the role of primary light source—is a conservative one. First, it is plausible that during evening twilight the very first appearance of a lunar halo is easily missed, which causes a systematic shift in the solar depression angle of the dots of Fig. 8 toward the right. For halos during eclipses such an effect does not occur, as the persistence of a halo at the transition to from pretotality to totality is easily verified. Second, a halo like the parhelion is usually more light intensive than the 22° halo and therefore has an even better chance to persist during totality. A parhelion is easy to monitor during the transition to totality, but because of its small size is difficult to find during twilight.

U. Hennig is acknowledged for preprocessing the halo data of the AKM.

References and Notes

1. W. E. Sharp, S. M. Silverman, and J. W. F. Lloyd, "Summary of sky brightness measurements during eclipses of the Sun," Appl. Opt. **10**, 1207–1210 (1971).
2. S. M. Silverman and E. G. Mullen, "Sky brightness during eclipses: a review," Appl. Opt. **14**, 2838–2843 (1975).
3. B. S. Dandekar, "Measurements of the zenith sky brightness and color during the total solar eclipse of 12 November 1966 at Quehua, Bolivia," Appl. Opt. **7**, 705–710 (1968).
4. G. E. Shaw, "Sky brightness and polarization during the 1973 African eclipse," Appl. Opt. **14**, 388–394 (1975).
5. H. R. Blackwell, "Contrast thresholds of the human eye," J. Opt. Soc. Am. **36**, 624–643 (1946).
6. E. S. Lamar, S. Hecht, S. Shlaer, and C. D. Hendley, "Size, shape, and contrast in detection of targets by daylight vision. I. Data and analytical description," J. Opt. Soc. Am. **37**, 531–545 (1947).
7. S. Hecht, "Visual thresholds of steady point sources of light in fields of brightness from dark to daylight," J. Opt. Soc. Am. **37**, 59 (1947).
8. R. Tousey and E. O. Hulburt, "Brightness and polarization of the daylight sky at various altitudes above sea level," J. Opt. Soc. Am. **37**, 886–896 (1947).
9. R. Tousey and E. O. Hulburt, "The visibility of stars in the daylight sky," J. Opt. Soc. Am. **38**, 177–183 (1948).
10. H. F. Weaver, "The visibility of stars without optical aid," Publ. Astron. Soc. Pac. **59**, 232–242 (1947).
11. M. J. Koomen, C. Lock, D. M. Packer, R. Tousey, and E. O. Hulburt, "Measurements of the brightness of the twilight sky," J. Opt Soc. Am. **42**, 353–355 (1952).
12. R. Tousey and M. J. Koomen, "The visibility of stars and planets during twilight," J. Opt. Soc. Am. **43**, 177–183 (1953).
13. K.-P. Möllmann and M. Vollmer, "Measurements and predictions of the illuminance during a solar eclipse," Eur. J. Phys. **27**, 1299–1314 (2006).
14. C. W. Allen, *Astrophysical Quantities* (Athlone, 1976).
15. G. T. Fechner, *Elemente der Psychophysik Teil II, Kapitel 16* (Breidkopf und Härtel, 1860); English translation from 1912 edition, http://psychclassics.yorku.ca/Fechner/.
16. L. Cowley, Atmospheric Optics website master, atoptics@gmail.com (personal communication, 2006).
17. A. Meinel and M. Meinel, *Sunsets, Twilights, and Evening Skies* (Cambridge U. Press, 1983).
18. W. E. Sharp, J. W. F. Lloyd, and S. M. Silverman, "Zenith intensity and color during the total solar eclipse of 22 July 1963," Appl. Opt. **5**, 787–792 (1966).
19. E. H. Carman, R. J. Skinner, and M. P. Heeran, "Zenith sky brightness and airglow emissions during the equatorial solar eclipse of 30 June 1973," Appl. Opt. **20**, 778–785 (1981).
20. L. Cowley, "Eclipse, Turkey March 29, 2006," http://www.atoptics.co.uk/ecl/eclipse.htm.
21. M. Vollmer and K.-P. Möllmann, "Total eclipse aficionados seek out the best observational spots," Phys. Educ. **41**, 193–195 (2006).
22. J. F. den Tonkelaar, *Het Strandweer*, KNMI Scientific Report WR 72–10 (1972); see also G. P. Können, *Het weer in Nederland* (Thieme Zutphen, 1983), pp. 57–58, available from KNMI, P. O. Box 201, 3730 AE De Bilt, The Netherlands.
23. An Occasional Correspondent (anon.), "A solar Eclipse, the approaching astronomical event: an observer's past experience," *New York Times*, 28 March 1875; see http://query.nytimes.com/gst/abstract.html?res=9E01E2D91439E43BBC4051DFB566838E669FDE.
24. See, for instance, M. Loomish Todd, http://www.exploratorium.edu/eclipse/1896.html; J. van der Weerd, R. Wenmaekers, and M. de Wit, "Het licht tijdens het verloop van de verduistering," Zenit **33**, 14–19 (2007).
25. The bluish tinge was also noted by G. P. Können in Madrid during the 2005 annular eclipse. It started during the deep-partial phase, persisted throughout the full 4 min of the annular phase, but disappeared shortly after third contact.
26. The bureau of the Royal Netherlands Association for Meteorology and Astronomy received several reports mentioning an "eerie metal-like twilight" at the maximum obscuration of the 1999 European eclipse, which was deep partial (>0.9) all over the Netherlands.
27. D. A. Velasques, "Zenith sky brightness and colour change during the total solar eclipse of 12 November 1966 at Santa Ines, Peru," Appl. Opt. **10**, 1211–1214 (1971).
28. E. Herranen, "Total Solar Eclipse in Turkey 29.03.2006," http://www.ursa.fi/~mellon/aurinko/index2006_en.shtml.

29. S. A. Mitchell, *Eclipses of the Sun* 5th ed. (Columbia U. Press, 1951).
30. M. Waldmeier, *Ergebnisse und Probleme der Sonnenforschung* (Becker & Erler, 1941).
31. F. K. Richtmyer, "The 'total light' of the solar corona," in *US Navy Solar Eclipse Expedition of 1937 to Canton Island,* , National Geographic Society Technical Papers, Solar Eclipse Series No. 1 (National Geographic Society, 1939), pp. 10–16.
32. R. van Dorland, *Video-Recording with Fixed Diaphragm of the 1999 European Solar Eclipse*, private recording (1999), Rob .van.Dorland@knmi.nl.
33. B. S. Dandekar and J. P. Turtle, "Day sky brightness and polarization during the total solar eclipse of 7 March 1970," Appl. Opt. **10**, 1220–1224 (1971).
34. J. W. F. Lloyd and S. M. Silverman, "Measurements of the zenith sky intensity and spectral distribution during the solar eclipse of 12 November 1966 at Bage, Brazil, and on an aircraft," Appl. Opt. **10**, 1215–1219 (1971).
35. C. S. Deehr and M. H. Rees, "The eclipse of 20 July 1963 spectrophotometry of atmospheric emissions," Planet. Space Sci. **12**, 875–888 (1964).
36. C. C. Batchelder, K. Batchelder, R. Hargreaves, and J. Hargreaves, "The total eclipse of the Sun, February 25, 1952 light-curve near mid-eclipse," Astrophys. J. **123**, 9–13 (1956).
37. R. A. Richardson and E. O. Hulburt, "Solar illumination and zenith sky brightness during the total solar eclipse of May 20, 1947," J. Geophys. Res. **54**, 229–238 (1949).
38. E. de Bary, K. Bullrich, and D. Lorenz, "Messungen der Himmelsstrahlung und deren Polarisationgrad während der Sonnenfinsternis am 15.2.1961 in Viareggio (Italien)," Geofis. Pura Appl. **48**, 193–198 (1961).
39. G. E. Shaw, "Sky radiance during a total solar eclipse: a theoretical model," Appl. Opt. **17**, 272–276 (1978).
40. G. P. Können, "Skylight polarization during a total eclipse: a quantitative model," J. Opt. Soc. Am. A **4**, 601–608 (1987).
41. C. Emde and B. Mayer, "Simulation of solar radiation during a solar eclipse: a challenge for radiative transfer," Atmos. Chem. Phys. **7**, 2259–2270 (2007); http://www.atmos-chem-phys.net/7/2259/2007/acp-7-2259-2007.pdf.
42. S. D. Gedzelman, "Sky color near the horizon during a total solar eclipse," Appl. Opt. **14**, 2832–2837 (1975).
43. F. Espenak, "NASA Eclipse Web Page," http://eclipse.gsfc.nasa.gov/eclipse.html.
44. W. N. Hall, "Spectral changes in the zenith skylight during total solar eclipses," Appl. Opt. **10**, 1225–1231 (1971).
45. H. A. Pohn, H. W. Radin, and R. L. Widley, "The Moon's photometric function near zero phase angle from Apollo 8 photography," Astrophys. J. **157**, L193–L195 (1969).
46. H. A. Pohn, H. W. Radin, and R. L. Widley, "Theoretical photometry," in *Analysis of Apollo 8 Photography And Visual Observations*, NASA SP-201, 40–41 (NASA,1969).
47. E. A. Whitacker, "An investigation of the lunar heiligenschein," in *Analysis of Apollo 8 Photography and Visual Observations*, NASA SP-201, 38–40 (NASA,1969).
48. S. J. O'Mearn, "Strange Eclipses," Sky Telesc. **98**, 116–120 (1999).
49. A. van der Salm, *Video-Recording of the 1991 Mexican Solar Eclipse*, personal recording (1991), salm0110@planet.nl.
50. C. M. Botley, "Lunar rainbow," Weather **25**, 287–288 (1970).
51. W. Hinz, "Die Sektion Halobeobachtung des AKM e.V.," http://www.meteoros.de/akm/akm2.htm.
52. G. P. Können and J. Tinbergen, "Polarimetry of a 22° halo," Appl. Opt. **30**, 3382–3400 (1991).
53. G. Rougier, "Photométrie photoélectrique globale the la lune," Ann. Obs. Strasb. **2**, 205–339 (1933).
54. E. W. Maunder, "The comet and the eclipse," Observatory **24**, 373–376 (1901).
55. C. Hinz and W. Hinz, "Die Halos im Januar 2005," Meteoros **9**, 70–75 (2006).
56. G. Stemmler, "50 Jahre Halobeobachtung 1953–2002," Meteoros **6**, 85–87 (2003).
57. S. Molau, "SHB halo key," http://www.molau.de/software/halo/halokey.pdf.